Investigation on the Dynamic Behavior of AlgoTuf 400F Steel

Part 1: Constitutive Strength Model

Geneviève Toussaint[1]

[1]Defence Research and Development Canada, Valcartier Research Center

2459 de la Bravoure Road, Québec (QC), Canada, G3J 1X5

Abstract

In order to improve finite element simulation predictions of a dynamic event such as a blast or a ballistic impact on a structure, the dynamic behavior of the materials involved has to be investigated. The information gathered from this investigation can then be further used to choose the constitutive material model as well as identified its parameters. In this paper, the main objective is to share the findings from this investigation for the AlgoTuf 400F steel. The first section of the paper presents the quasi-static test that were performed by Defence Research and Development Canada (DRDC) as well as the split Hopkinson pressure bar (SHPB) tests that were performed at a strain rate between 10^3 and 10^4 s^{-1}. These experimental data showed that at low strain rates, the material did not exhibit exactly the same behavior in the rolling direction (longitudinal direction) compared to the transverse one. It was also found that at higher strain rates, the effect of the manufacturing method on the properties through a 25.4 mm (one inch) thick plate could be neglected. Nevertheless, the material has showed sensitiveness to the strain rate and this was taken into consideration in the constitutive material model. In the second section, the plasticity parameters identified for the simplified Johnson-Cook constitutive strength model obtained using these experimental data are presented. The third section describes the 2D axisymmetric finite element (FE) model of the SHPB test and shows good agreement between numerical and experimental results. It was therefore possible in the last section to perform a parametric analysis to study the deformation response of an AlgoTuf 400F plate loaded by a spherical air blast using the particle blast method. The next step of this investigation will be to identify a constitutive damage/failure model and get its parameters to be able to predict accurately the deformation and damage/failure response of an AlgoTuf 400F steel plate subjected to a blast event.

Keywords: AlgoTuf, SHPB, Johnson-Cook, Finite element simulation, Air blast, Square plate, PBM.

1 Introduction

Over the years, finite element (FE) simulations have proven to be a very useful tool to guide experimental designs and settings. These numerical predictions are however sensitive to the material models and their parameters, and depend on the experiments performed to get them. Therefore, for defence applications involving the assessment of blast effects on a structure and considering that a blast is typically in the range of 10^2 to 10^4 s^{-1} [1], it is thus important beforehand to determine if the materials involved are strain rate sensitive, i.e. if their dynamic behaviour depends on their loading rates as this will influence the choice of the constitutive material model as well as their parameters. One way to do that is to conduct tests at different strain rates.

In this work, Defence Research and Development Canada (DRDC) was interested to initiate a thorough investigation on the dynamic behavior of AlgoTuf 400F steel [2]. This material, known to be high-strength and abrasion-resistant steel, has potential for different applications. Unfortunately, the state-of-the art on the dynamic behavior of AlgoTuf 400F steel is very limited in the literature. Bassim (2012) [3] and Bassim et al. (2015) [4] have published some results on the dynamic torsional Hopkinson tests as well as on direct impact tests on this material. These publications did not provide sufficient information to be able to fully understand the behavior and calibrate the constitutive model parameters. In order to fulfil this gap, the main objective of the current work is thereby to extend the

investigation as well as provide the plasticity parameters identified for the Johnson-Cook constitutive strength model [5, 6]. Therefore, the second section describes the specimen designs and experimental configurations of the quasi-static and split Hopkinson pressure bar tests and presents the results obtained. These results were used to determine the parameters of the simplified Johnson-Cook model. The third section presents a 2D axisymmetric finite element model of the split Hopkinson bar and the simulations conducted using the LS-DYNA hydrocode [7]. The numerical results are then compared to the experimental ones in order to validate the parameters obtained for the simplified Johnson-cook model. Finally, finite element simulations are performed using results from the previous section to study the deformation of a plate loaded by a spherical air blast using the particle blast method (PBM) [8, 9].

2 Quasi-static and split Hopkinson bar tests on AlgoTuf 400F

2.1 Quasi-static tests

For the quasi-static tests, the specimen were machined according to the ASTM E8 standard [10] and cut in the rolling (0°) and transverse (90°) directions of the plate, as shown in Figure 1. In total, eight tensile tests (4 in each direction) were performed using an Instron 5584 servo-mechanical machine and were performed at a constant crosshead velocity. The Instron machine is shown in Figure 2.
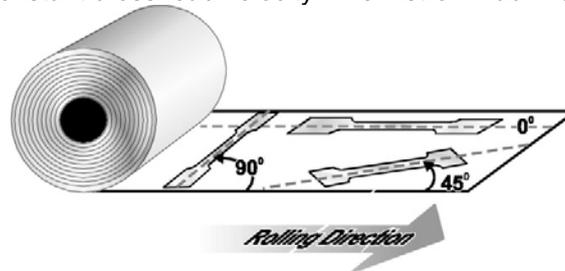

Fig.1:   Orientation of the specimens (rolling 0° and transverse 90°) [11].

Fig.2:   Instron 5584 machine.

The engineering stress-strain data were calculated using the conventional equations provided in [10], i.e. the engineering strain (ε_e) was given by equation 1:

$$\varepsilon_e = \frac{GL - GL_0}{GL_0} \tag{1}$$

where GL was the gage length of the specimen and GL_0 was the original gage length. The engineering stress (σ_e) was given by :

$$\sigma_e = \frac{P}{A_0} \tag{2}$$

where P was the force applied on the specimen and A_0 was the original cross sectional area of the specimen. The engineering stress-strain curves obtained for all the specimens are shown in Figure 3.
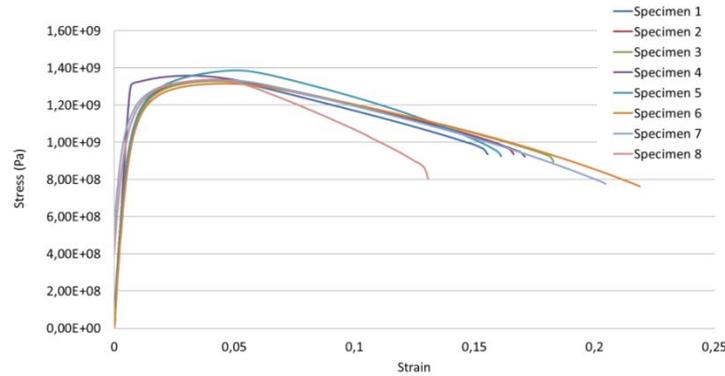
Fig.3:   Quasi-static engineering stress-strain curves of AlgoTuf 400F specimens.

Table 1 provides the mean of the maximum tensile stress and strain at failure for each group of specimens.

	Longitudinal Mean (1 to 4)	Transverse Mean (5 to 8)
Maximum Tensile Stress (MPa)	1340	1327
Strain at failure (%)	16.9	17.9

Table 1: AlgoTuf 400F quasi-static properties.

As can be seen in Table 1, in the longitudinal direction the maximum tensile stress is slightly higher while the failure strain is slightly lower.

In order to convert the engineering stress/strain curves in true stress/strain curves, data were analysed before and after the necking. First, until the onset of necking, the true strain (ε) and true stress (σ) were given by the following formulations [10]:

$$\varepsilon = \ln\left(\frac{GL}{GL_0}\right) \tag{3}$$

$$\sigma = \frac{P}{A_0}\left(\frac{GL - GL_0}{GL_0} + 1\right) \tag{4}$$

And assuming that the necking begun at maximum load, beyond the maximum load the true strain and stress were defined by $\varepsilon = \ln(A_0/A)$ and by $\sigma = P/A$ where A was the actual instantaneous cross sectional area of the specimen. The true fracture strain was then given by equation 5 [10]:

$$\varepsilon_f = \ln\left(\frac{A_0}{A_f}\right) \tag{5}$$

The final cross sectional area (A_f) of the specimen was measured after the test by joining the corresponding broken specimen back together. The true fracture stress (σ_f) was determined using equation 6:

$$\sigma_f = \frac{P_f}{A_f} \tag{6}$$

The final load at fracture (P_f) was obtained from the experimental data. According to [10], when the cross-head velocity (v) of the testing machine is constant, the true strain rate decreases as the specimen elongates. Therefore, using equation (7), only the engineering strain rate $\dot{\varepsilon}_e$ is calculated for the quasi-static data:

$$\dot{\varepsilon}_e = \frac{v}{GL_0} \tag{7}$$

Figure 4 presents the true stress-strain curves obtained for the AlgoTuf 400F in the longitudinal (specimen 1 to 4) and transverse (specimen 5 to 8) directions.
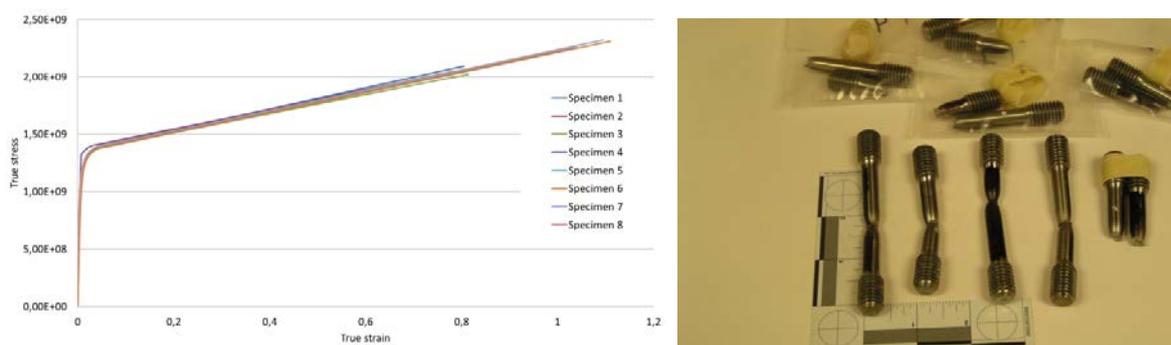

Fig.4: True stress-true strain curves obtained in the longitudinal and transverse directions for AlgoTuf 400F(left), examples of broken specimens (right).

It was found that the specimens machined in the transverse direction showed a higher true strain at failure. However, since the failure strain was not considered in this study, the quasi-static properties were assumed homogenous in both directions.

2.2   Split Hopkinson pressure bar tests

The Hopkinson bar testing technique has evolved over the years and is now used by many researchers studying the dynamic behavior of materials. As presented in Gama et al. [12], this progress in the development and theory of high strain rate testing of materials begun with a researcher named John Hopkinson in 1872, which was doing stress wave experiments in iron wires. It was followed by experiments in 1905 by his son Bertram Hopkinson who developed later the pressure bar technique in 1914. Then, in 1941 Bancroft proposed a solution to the frequency equation for the velocities of longitudinal waves in cylindrical bars. In 1948, Davies reported some limitations of the pressure bar technique. In 1949, Kolsky developed the 1D pressure bar data analysis technique and the experimental method. His systems was later known as the Kolsky bar or SHPB. Nemat-Nasser et al. [13] invented in 1991 a method to trap the pulses at the end of the bars. A more detailed historical background of the Hopkinson bar experimental technique can be found in [12, 13]. Nowadays, the progress still continues and a considerable amount of efforts is invested by many researchers to use and adapt the Hopkinson bar technique to characterise their materials and validate their material models [14, 15, 16, 17, 18, 19, 20, 21].

One advantage of the split Hopkinson bar technique is that it can achieve the highest uniform uniaxial stress loading of a specimen in compression. At the Valcartier Research Center, the split Hopkinson pressure bars (SHPB) set-up, illustrated in Figure 5 (left), has proven to be successful to characterize materials under high strain rate [21, 22, 23, 24]. The classical operation of the SHPB is to propagate an elastic wave in the bars by impacting the incident bar with a striker. Since this wave is assumed to propagate in one dimension only, the specimen, sandwiched between the incident and transmitted bar, is considered to deform uniformly (i.e. stress and strain are uniform along its length as a function of time). This assumption is suitable only if several conditions are respected. They are well explained in several publications [10, 21]. As well, when performing test with the SHPB system, the accuracy

and the precision of the entire data acquisition chain and the analysis software are of primary importance and were evaluated previously [24]. The calibration and verification of all the following components of the system led to improved and control of the test results: strain gage accuracy (strain gage alignment, strain gage transverse sensitivity, strain gage positioning distance, strain gage factor, strain gage length selection, strain gage bridge nonlinearity, evaluation of 'actual' strain, non-linearity and non-reciprocity in shunt calibration) and data acquisition chain accuracy (sampling theorem, anti-aliasing filter, expected signal spectrum content), on-board static calibration, on-board dynamic calibration and striker impact speed accuracy. A schematic diagram of the SHPB set-up is provided in Figure 5 (right).
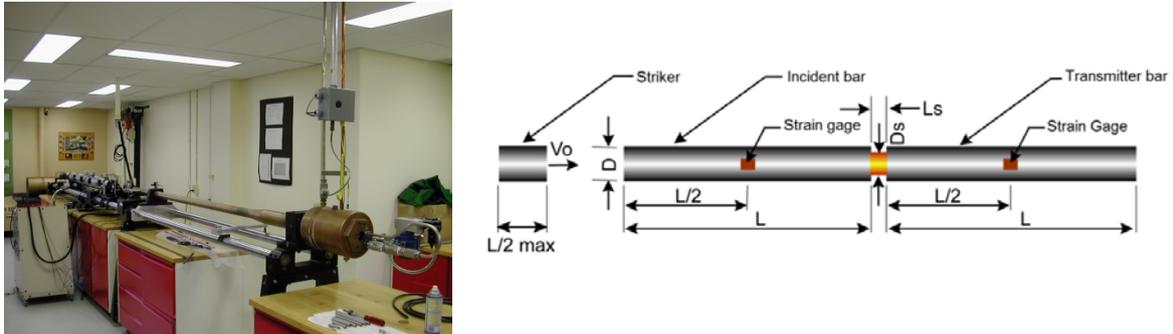

Fig.5:   DRDC SHPB set-up (left), Schematic diagram of the SHPB set-up (right).

The incident and transmitter bars had a length of 800 mm with a diameter of 14.5 mm while the striker had a length of 200 mm. The bars and the striker were made from Maraging Steel while the specimen tested was made of AlgoTuf 400F. The mechanical properties are provided in Table 2.

	ρ kg/m^3	E GPa	σ_u GPa	c^a m/s	υ	Z^b kg/s
Maraging Steel	8064	182	2.618	4751	0.33	6326
AlgoTuf 400F	7870	210	1.206^c	5166	0.33	1150
[a]the longitudinal wave velocity c was calculated using $c = \sqrt{E/\rho}$ [25].						
[b]the impedance Z was given by $Z = \rho A c$ [26] where *A* was the cross sectional area.						
[c]data obtained from [2].						

Table 2: Mechanical properties of the bars, the striker and the specimen.

The nominal specimens' dimensions of 6 mm (diameter) x 3 mm (length) were determined from theoretical calculation and considering the time required to achieve stress equilibrium in the specimen. More details on how to determine and optimize the specimen dimensions are provided in [21, 22].

In order to get an insight of the rolling effect on the material properties through the 25.4 mm (1 inch) thick plate, hardness measurements were taken at every 2.54 mm through the thickness of the plate using the Rockwell scale A. Results are given in Table 3.

Distance from top surface (mm)	2.54	5.08	7.62	10.16	12.7	15.24	17.78	20.32	22.86
Hardness (HRA)	72.3	71.9	71.6	71.8	72.0	71.6	71.5	71.8	72.2
Mean: 71.9 and Standard deviation: 0.3									

Table 3: Hardness measurements

By looking at this table, it is expected that the material will behave homogenously through the thickness. This hypothesis was confirmed by comparing the results from tests conducted at

approximately 20 m/s using the SHPB apparatus, for five specimens that were machined in the direction perpendicular to the surface of the plate. The comparison of the specimen true stress - strain response is presented in Figure 6. The quasi-static data obtained in the previous section is also presented in this figure and allows to demonstrate the stress strain sensitiveness of the material.
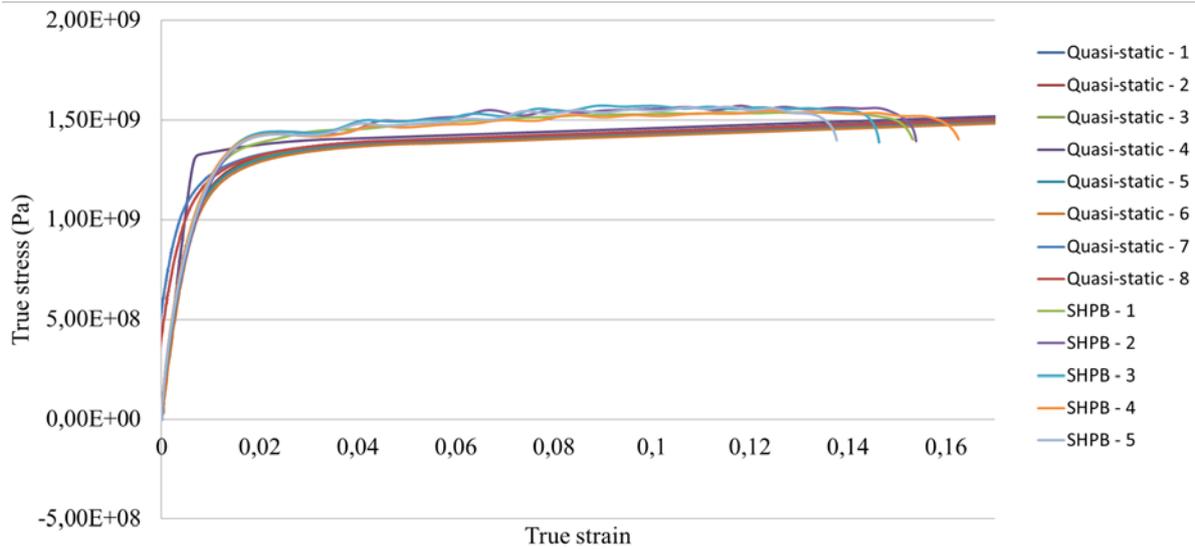

Fig.6:   *Specimens true stress – strain response obtained with quasi-static and SHPB tests.*

Test Number	Impact Velocity m/s	Nominal Strain[a] Rate ($\dot{\varepsilon}_n$) s^{-1}	D_0 mm	D_f mm	l_0 mm	l_f mm
1	20.60	1584	6.03	6.60	3.00	2.60
2	20.45	1578	6.01	6.48	3.01	2.61
3	20.15	1465	6.01	6.46	3.00	2.63
4	20.61	1504	6.02	6.53	3.00	2.62
5	19.50	1386	6.01	6.41	3.00	2.65
Mean	**20.26**	**1503**	**6.02**	**6.50**	**3.00**	**2.62**

[a]The nominal strain rate is given by $\dot{\varepsilon}_n = \dfrac{\varepsilon_n c_b}{2 L_0}$ where $\varepsilon_n = \left| \dfrac{l_f - l_0}{l_0} \right|$, c_b is the longitudinal wave velocity in the pressure bars, L_0 is the striker length (200 mm) and l_0 and l_f are the initial and final length of the specimen respectively.

Table 4: Initial and final specimen dimensions.

3 Constitutive material models and constants determination

It was concluded previously that the Algotuf 400F material exhibited sensitivity to the strain rates; this behavior has therefore to be accounted for in the choice of the constitutive material model. In the literature, several constitutive material models including strain rates effects are available, such as Cowper and Symonds, Johnson and Cook, Zerilli and Armstrong, Moudlin et al. and they are all explained in the user's manual [27] and implemented in the Ls-Dyna software. In this work, the simplified version of the Johnson Cook material model was used for its simplicity to get the material parameters. The Johnson-Cook equation is provided below [5].

$$\sigma_y = \left(A + B \varepsilon^n \right)\left(1 + C \ln \dot{\varepsilon}^* \right)\left(1 - T^{*m} \right) \qquad (8)$$

Where A is the yield stress, B and n represents the effects of strain hardening, ε is the effective plastic strain, C accounts for the effect of strain rate, $\dot{\varepsilon}^*$ is given by $\dot{\varepsilon}/\dot{\varepsilon}_0$ where $\dot{\varepsilon}$ is the strain rate, $\dot{\varepsilon}_0$ is the reference strain rate, m is the thermal softening factor and $T^* = (T-T_r)/(T_m-T_r)$ where T_m is the melting temperature of the material and T_r is the room temperature. In the simplified model however, thermal effects are not considered, therefore a preliminary set of data was determined for A, b, n and C parameters only. These parameters are provided in Table 5 and are evaluated using finite element simulations in the next section.

	A GPa	B MPa	n	C	$\dot{\varepsilon}_0$ 1/s
AlgoTuf 400F	1.1263	569.3235	0.2459	0.004525	0.0005

Table 5: Simplified Johnson-Cook model parameters.

The selection of $\dot{\varepsilon}_0$ was consistent with the choice made previously for parameters A and B [28] and was calculated using equation (7).

4 Verification and Validation of the material model

In this section, a verification and validation of the constitutive model and the parameters was accomplished by reproducing the SHPB test of an AlgoTuf 400F specimen using finite element simulations and by comparing the experimental and numerical results together.

The finite element model of the SHPB, shown in Figure 7, was reflected on the central axis to provide an entire view. A larger view of the specimen that was sandwiched between the bars is also presented. A mesh sensitivity study was performed previously on the incident and transmitter bars and on the striker and was detailed in [23]. The same mesh sizes were used for the SHPB configurations, i.e. the striker was meshed with 3,000 elements having the following dimensions 0.477 mm x 0.995 mm, while the incident and transmitter bars were meshed with 28,320 elements having a coarser and finer region with the following element dimensions of 0.483 mm x 1.0 mm and 0.161 mm x 0.140 mm respectively. Finally, the specimen had a diameter of 6.10 mm and a length of 3.01 mm. The 2D axisymmetric model was modeled with 760 shell elements having 0.1525 mm x 0.0792 mm.
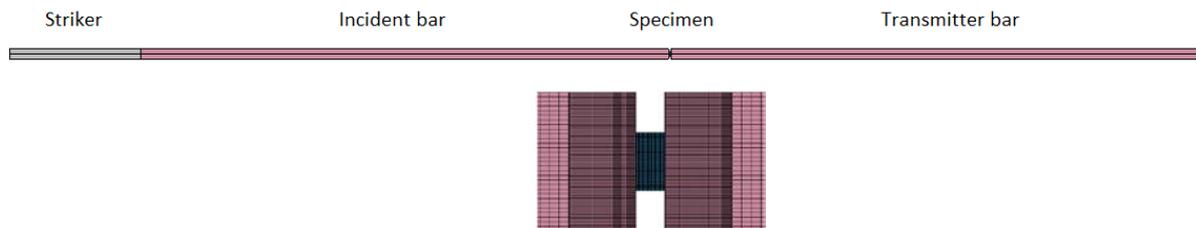

Fig.7: FE model of the SHPB revolve around the center axis.

The striker, the incident and transmitter bars made of Maraging steel were defined by an elastic material model since these parts were assumed to behave only elastically. The specimen made of AlgoTuf 400F was defined by the simplified Johnson-cook material model. The mechanical properties of these two materials and parameters are provided in Table 2 and Table 5. A contact 2D automatic surface to surface was defined between the lagrangian parts. An initial nominal velocity of 20.26 m/s was given to the striker. Finally, simulations were run with LS-DYNA version 9 and four processors. Figure 8 shows a sequence of the specimen deforming as a function of time.
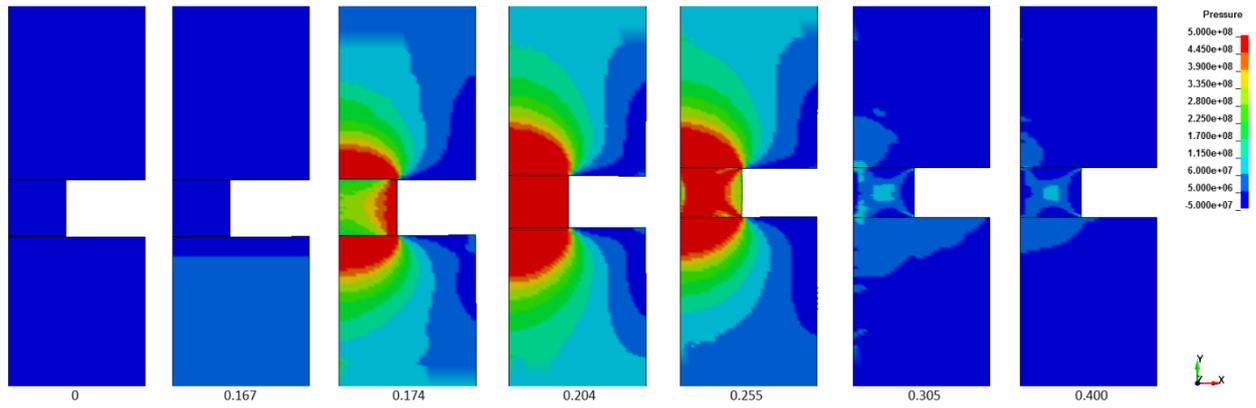
Fig.8: Deformation sequence of the specimen as a function of time (ms).

Figure 9 shows that the stress time histories of the elements located at the same location than the gages mounted on the incident and transmitter bars compare well with experimental data. For comparison purpose, the numerical results were shifted in time.
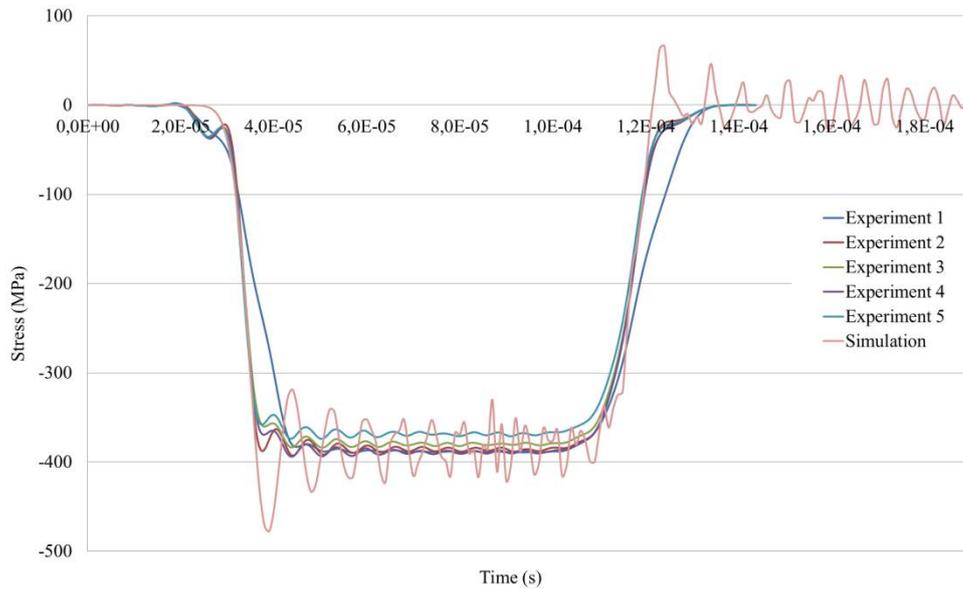

Fig.9: Stress obtained at the gages location on the incident and transmitter bars, as a function of time, compared to the numerical results.

The experimental true stress and the effective plastic strain in the specimen were determined according to procedure explained in [29]. Figure 10 compares the numerical simulations to the experimental true stress – effective plastic strain response of AlgoTuf 400F specimens.
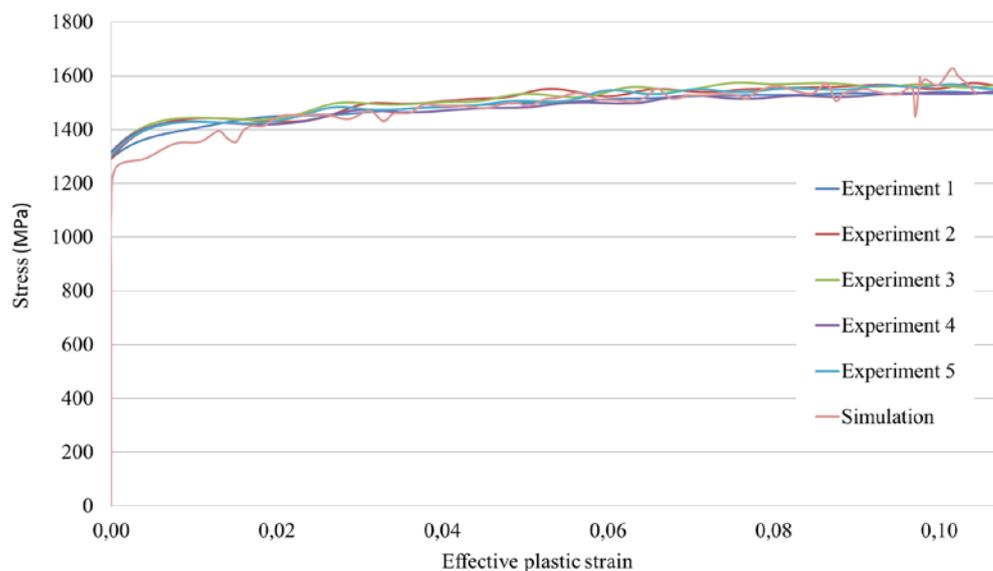
Fig.10:   Specimen true stress - effective plastic strain response compared to the numerical results.

The numerical results observed are close to the experimental data. Table 6 provides the initial and final experimental mean diameters and lengths of the specimens and the numerical results.

	Impact Velocity (m/s)	Nominal Strain Rate	D_0 (mm)	D_f (mm)	l_0 (mm)	l_f (mm)
Experimental mean	20.26	1503	6.02	6.50	3.00	2.62
Numerical	20.26	1503	6.10	6.48	3.01	2.67
Relative Error[a] (%)				0.3		1.9

[a] The relative error is calculated using: $|((D_{fe}-D_{fn})/D_{fe})|$ and $|((L_{fe}-L_{fn})/L_{fe})|$

Table 6: Comparison of the initial and final experimental mean diameters and lengths to numerical results.

By looking at the very small relative error and considering the good agreement that was obtained between the experiment and numerical results, the plasticity parameters identified for the simplified Johnson-Cook constitutive strength model for the AlgoTuf 400F are validated.

5 Application

The next phase of this work was to perform a numerical analysis of a square AlgoTuf 400F plate subjected to an impulsively spherical blast load. The main objective was to investigate the deformation response of the plate by varying the stand-off distances and charge masses in order to determine the combination to be used in the future experiments to get a noticeable mid-point deflection. The finite element model, shown in Figure 13, is thus a simplified version of the already existing experimental small scale set-up of a pendulum [30], shown in Figure 14. The FE model consists of a plate clamped between the main and the rigid frames.
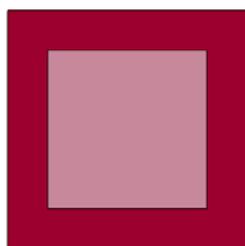
Fig.11: Finite element model of the simplified set-up (left), Experimental small scale set-up (right) [30].

The same simplified model of the experimental set-up as explained in [21, 31] is used in this work. A mesh sensitivity analysis was already conducted [31] where the main frame was modeled with 11,616 hexahedron elements of 2.12 mm x 2.12 mm and 1.1 mm thick while the rigid frame was modeled with 61,992 hexahedron elements having 2.12 mm x 2.12 mm and 2 mm thick. In this work, the plate has a thickness of 4.7625 mm and is made of AlgoTuf 400F. The constitutive model parameters that were developed in the previous sections and presented in Table 5 were used for the steel. Table 7 provides the parameters for the main and the rigid frames made of A514 steel. A contact automatic surface-to-surface was defined between the parts.

	ρ kg/m^3	E GPa	υ
A514	7850	205	0.29

Table 7: Properties of the rigid and main frames [32]

Previous studies [8, 9, 21] have demonstrated the accuracy of the particle blast method [27] to reproduce using finite element simulations the effects of a spherical air blast on a plate. This same method was used in this work. The number of air particles was set to 1,180,000 as suggested by Toussaint and Bouamoul [21] while the number of explosive particles was calculated to get, as suggested by Teng [9], an equal mass for the air and explosive particles. The stand-off distance was defined as the distance between the surface of the plate center and the center of the charge. The simulations were run with LS-DYNA version 9 and four processors. Table 8 provides the results from this parametric analysis.

Explosive mass (g)	Number of particles	Stand-off distances (mm)	Mid-point deflection (mm)
50	40836	100	-
100	81672	100	~2
150	122508	100	7
250	204180	100	19
300	245016	100	23
350	285852	100	26
400	326688	100	30
450	367524	100	34
500	408361	100	37
150	122508	200	-
200	163344	200	~1
300	245016	200	~4
400	326688	200	10
500	408361	200	15
750	612542	200	24
1000	816722	200	32

Table 8: Parametric Analysis.

Table 8 shows that for the 100 mm and 200 mm stand-off distances, at least 250 g and 500 g of C-4 should be use respectively to get a noticeable mid-point deflection. An example of the deflection of the plate as a function of time for a stand-off distance of 100 mm and a C-4 mass of 400 g is shown in Figure 12.
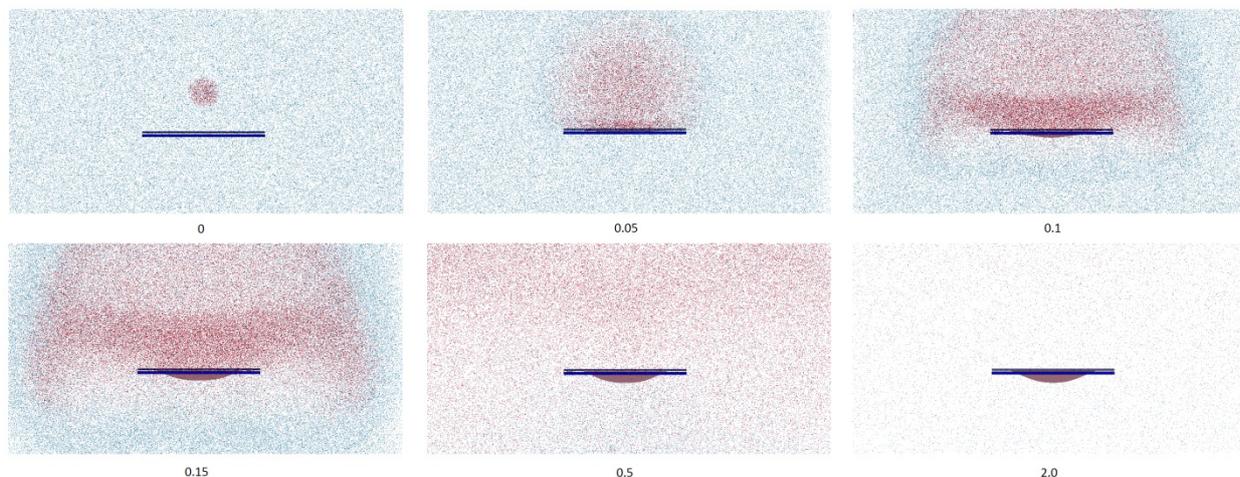

Fig.12:   Deformation sequence of an AlgoTuf 400F steel plate as a function of time (ms) for 100 mm stand-off distance and 400 g of C-4 mass.

The finite element simulations conducted in this section allowed to investigate numerically the deformation response of a plate made of AlgoTuf 400F by varying the stand-off distances and charge masses. The data generated will be used to optimise the experimental matrix of the experiments to be carried out. As well, the FE model developed can be used in the future to predict the deflection of an AlgoTuf 400F steel plate.

6 Summary

In this paper, the main objective was to share the findings from an investigation on the dynamic behavior of AlgoTuf 400F steel. It was found from the quasi-static tensile tests that the specimens machined in the transverse direction showed a higher true strain at failure. However, for the purpose of this study, the quasi-static properties were assumed to be homogenous in both directions. Results obtained from the experiments performed on a split Hopkinson pressure bar (SHPB) results also demonstrated that at high strain rates the effect of the rolling on the properties through the thickness of the plate could be neglected. Nevertheless, the AlgoTuf 400F material has showed sensitiveness to the strain rate. This was confirmed by comparing the quasi-static tests to the SHPB tests. The plasticity parameters determined for the simplified Johnson-Cook constitutive strength model were obtained using these experimental data and were validated by reproducing the SHPB test of an AlgoTuf 400F specimen using finite element simulations. This constitutive model was then used to investigate, using finite element simulations, the deformation response of a plate made of AlgoTuf 400F by varying the stand-off distances and charge masses. The data generated demonstrated that for the 100 mm and 200 mm stand-off distances, at least 250 g and 500 g of C-4 should be use respectively to get a noticeable mid-point deflection. The data generated will be used to optimise the experimental matrix of the experiments to be carried out. As well, the FE model developed can be used in the future to predict the deflection of an AlgoTuf 400F steel plate. Finally, the next step of this investigation will be to identify a constitutive damage/failure model and get its parameters to be able to predict accurately the deformation and damage/failure response of an AlgoTuf 400F steel plate subjected to a blast event.

7 Acknowledgements

8 Literature

[1]   Ngo T., Mendis P., Gupta A. and Ramsay J.: "*Blast Loading and Blast Effects on Structure An Overview*", EJSE Special Issue: Loading on Structures, 2007.

[2]   http://www.essarsteelalgoma.com/

[3]   Bassim M. N.: "*Torsional Hopkinson Testing, AlgoTuf 400F*", DRDC Valcartier CR 2011-060, 2012.

[4]   Bassim N., Boakye-Yiadom S., Toussaint G. and Bolduc M.: "*Characterization of the Dynamic Behaviour of AlgoTuf Armour Steel during Impact and in Torsion*", EPJ Web of Conferences 94, 2015, 02005-p.1-6.

[5]   Johnson G.R. and Cook W. H.: "*A constitutive model and data for metals subjected to large strains, high strain rates and high temperatures*", Proc. 7th International Symposium on Ballistics, 1983, p.541-547.

[6]   Johnson G.R. and Cook W. H.: "*Fracture Characteristics of Three Metals subjected to Various Strains, Strain Rates, Temperatures and Pressures*", Engineering Fracture Mechanics Vol. 21. No.1, 1985, p.31-48.

[7]   LSTC, Livermore Software Technology Corporation, www.lstc.com

[8]   Teng H. and Wang J.: "*Particle Blast Method (PBM) for the simulation of Blast Loading*", Livermore Software Technology Corporation, 13th International LS-DYNA Users Conference. 2015.

[9]   Teng H.: "*Coupling of Particle Blast Method (PBM) with Discrete Element Method for buried mine blast simulation*", Livermore Software Technology Corp. 14th International LS-DYNA Users Conference, 2016.

[10]   ASM Handbook. *Volume 8 Mechanical Testing and Evaluation*, 2000.

[11]   https://www.google.ca/search?q=specimen+rolling+direction&safe=active&biw=1920&bih=91 2&source=lnms&tbm=isch&sa=X&ved=0ahUKEwjy8LSsnLjSAhWHvBoKHdF5DPUQ_AUIBig B#safe=active&tbm=isch&q=rolling+direction&*&imgrc=UE7suSYbaRPy_M:

[12]   Gama B.A., Lopatnikov S. L. and Gillespie Jr J. W.: "*Hopkinson bar experimental technique: A critical review*", App. Mech. Rev. vol.57 no4, 2004.

[13]   Nemat-Nasser S., Isaacs J. B. and Starrett J. E.: "*Hopkinson Techniques for Dynamic Recovery Experiments*", Proceedings: Mathematical and Physical Sciences, Vol.435, Issue 1894, 1991, p.371-391.

[14]   Lesuer D.R., Kay G.J and LeBlanc M. M.: "*Modeling Large-Strain, High-Rate Deformation in Metals.* Lawrence Livermore National Laboratory. UCRL-JC-134118, 2001.

[15]   Marais S. T., Tait R. B., Cloete T. J. and Nurick G.N.: "*Material testing at high strain rate using the split Hopkinson pressure bar*", Latin American Journal of Solids and Structures 1, 2004, p. 319-339.

[16]   Seo S., Min O., Yang H.: "*Constitutive equation for Ti-6Al-4V at high temperatures measured using the SHPB technique*", International Journal of Impact Engineering 31, 2005, p.735-754.

[17]   Manes A., Peroni L., Scapin M. and Giglio M.: "*Analysis of strain rate behavior of Al 6061 T6 Alloy*", Procedia Engineering 10, 2011, p.3477-3482.

[18]   Berkovic L., Chabotier A., Coghe F. and Rabet L.: "*Constitutive equations of a ballistic steel alloy as a function of temperature*", EPJ Web of Conferences 26, 2012, p04017-p.1-4.

[19]   Church P. Cornish R, Cullis I., Gould P. and Lewtas I. *Using the split Hopkinson pressure bar to validate material models.* Royal Society Publishing, 2014.

[20]   Gilioli A., Manes A., Giglio M. and Wierzbicki T. *Predicting ballistic impact failure of aluminium 6061-T6 with the rate-independent Bao-Wierzbicki fracture model.* International Journal of Impact Engineering 76, 2015, p.207-220.

[21] Toussaint G. and Bouamoul A.: "*Close-Range Blast Effects on Small Square Clamped Plates Made from Aluminum 6061-T6*", Journal of Dynamic Behavior of Materials, 3(1), 2017, p.83-99. DOI: 10.1007/s40870-017-0096-4.

[22] Bolduc M.: "*Split Hopkinson Bar Experiment: Aluminium 6061-T6*", Defence Research and Development Canada, TM 2004-362, 2005, Unclassified.

[23] Bouamoul A.: "*2D Hopkinson Bar Simulation analysis, Al 6061-T6 Specimen*", Defence Research and Development Canada, TM 2004-363, 2006, Unclassified.

[24] Bolduc M. and Arsenault R.: "*Improving accuracy in SHPB*", Defence Research and Development Canada, TM 2005-380, 2008, Unclassified.

[25] Gallager, P.J: "*Split Hopkinson Pressure Bar Apparatus Overview and Simple Analysis*", Defence Research and Development Canada. DREV M-3048/90, 1990, Unclassified.

[26] Kaiser M. A.: "*Advancements in the Split Hopkinson Bar Test*", Thesis submitted to the Faculty of the Virginia Polytechnic Institute and State University, 1998.

[27] LSTC *LS-DYNA Keyword User's Manual Vol. I, r6634.* Livermore Software Technology Corporation, 2015.

[28] Schwer L.: "*Optional Strain-Rate Forms for the Johnson Cook Constitutive Model and the Role of the Parameter Epsilon_0*", 6th European LS-DYNA User's Conference, 2007.

[29] http://ftp.lstc.com/anonymous/outgoing/support/FAQ/stress_vs_strain_for_plasticity_models

[30] Bolduc M., Personal Communications.

[31] Fillion-Gourdeau F. and Bolduc M.: "*Numerical analysis of blast on aluminium plates Geometrical effects*", Defence Research and Development Canada, TR 2010-066, 2010, Unclassified.

[32] www.matweb.com